https://doi.org/10.5194/egusphere-2026-4760
Preprint. Discussion started: 21 August 2026

Irrigation Water Redistribution and Competition Mechanisms Between Cropland and Shelterbelts in Arid Regions: Insights from Stable Water Isotopes data

Xinyue Wang[1,2,3], Dongdong Qiu[6], Guofeng Zhu[1,2,3], Yuanfeng Liu[4,5], Rui Li[1,2,3], Zhijie Zheng[1,2,3], Ru Ma [1,2,3], Wenzhang Sun[1,2,3], Yaxin Li [1,2,3], Dongfei Yang [1,2,3], Yitian Lei[1,2,3]*

Affiliations:

[1] College of Geography and Environmental Science, Northwest Normal University, Lanzhou 730070, Gansu, China

[2] Shiyang River Ecological Environment Observation Station, Northwest Normal University, Lanzhou 730070, Gansu, China

[3] Lanzhou Sub-center of the Remote Sensing Application Center, Ministry of Agriculture and Rural Affairs (MARA), Lanzhou 730070, Gansu, China

[4] Institute of Soil and Water Conservation Science of Gansu Province, 730020, Lanzhou, China

[5] Soil and Water Conservation Engineering Research Center of Gansu Province, 730020, Lanzhou, China

[6] School of Atmospheric Sciences, Joint International Research Laboratory of Atmospheric and Earth System Sciences, Nanjing University, Nanjing 210023, China

** Corresponding author. Email: zhugf@nwnu.edu.cn,gfzhu@lzb.ac.cn.*

Abstract: Protective forests play an important role in maintaining the stability of arid oasis agroecosystems; however, water exchange and competition between shelterbelts and cropland under limited water availability remain poorly quantified. This study used stable hydrogen and oxygen isotopes to investigate irrigation-water redistribution and water-use interactions in a maize (*Zea mays* L.)–poplar (*Populus alba* L.) shelterbelt

https://doi.org/10.5194/egusphere-2026-4760
Preprint. Discussion started: 21 August 2026

system in the Minqin Oasis, Hexi Corridor. The results showed that irrigation water was transferred from cropland to shelterbelts through both soil lateral movement and root-mediated uptake. Across four irrigation events, modeled transpiration-related water exchange between farmland and shelterbelts reached 84.49 mm, accounting for 19.56% of applied irrigation water. Irrigation-induced lateral transfer into shelterbelt soil averaged 13.26% of irrigation depth, with the largest contribution occurring in the 20–60 cm soil layer (5.49%). Maize and poplar exhibited substantial overlap in water-source use, with a mean proportional similarity index of 73.35%, indicating strong potential competition for soil water resources. These findings reveal that irrigation water redistribution links cropland and shelterbelts through coupled hydrological processes and highlight the need to jointly consider crop water demand and shelterbelt water consumption in arid oasis management.

Keywords: Stable isotopes; Farmland–shelterbelt system; Plant water use; IsoSource

1. Introduction

Farmland shelterbelts enhance farmland biodiversity (Fischer et al., 2010; Tamburini et al., 2020) and can improve agroecosystem structure, reduce wind erosion, stabilize sand, ameliorate the farmland microclimate, protect crops, increase yields, and strengthen crop resistance to natural hazards (Kanzler et al., 2019; Shen et al., 2016; Xue et al., 2019). These deliberately established and managed systems form an important ecological component in oasis agriculture and help maintain agroecosystem stability. Previous studies have shown that shelterbelts can promote crop growth and yield by regulating the farmland microclimate and improving soil physical and chemical properties (Brandle et al., 2004; Iwasaki et al., 2019; Zheng et al., 2016). However, shelterbelts may also compete with crops for water, light, and nutrients; competition for water is especially important and may reduce crop productivity (Liu et al., 2020; Rivest and Vézina, 2015; Woodall and Ward, 2002).

Water is a primary limiting factor in arid and semi-arid ecosystems (Huang et al., 2007; Ren et al., 2016). It directly affects crop growth, development, and yield (Mueller et al., 2012; Rosa et al., 2020; Ward and Pulido-Velazquez, 2008) and constrains both

https://doi.org/10.5194/egusphere-2026-4760
Preprint. Discussion started: 21 August 2026

afforestation and the stability of farmland-shelterbelt systems. Previous studies have generally examined soil-water dynamics or plant water sources separately for shelterbelts and crops (Qiu et al., 2023a; Wang et al., 2023; Zhao and Zhao, 2014). Studies of coupled farmland-shelterbelt water relations have focused mainly on exchanges among landscape units (Yi et al., 2015; Zhang et al., 2016) or on plant water sources (Liu et al., 2018). Consequently, the relationship between crop-tree water competition and water exchange within farmland-shelterbelt systems remains insufficiently resolved. Some earlier studies used conventional approaches, including root surveys and HYDRUS-1D simulations. Root surveys are destructive and labor-intensive (Rothfuss and Javaux, 2017), whereas model-based estimates may carry substantial uncertainty (Tan et al., 2015). Stable hydrogen and oxygen isotopes provide tracers of hydrological connectivity, transformation, and recharge among water bodies (Bowen et al., 2019) and are increasingly used to quantify root water uptake and water-source partitioning in agricultural and agroforestry systems (Penna et al., 2020; Qiu et al., 2023b; Zhang et al., 2022). Recent isotope and labeling studies further show that plant water-use strategies and interspecific water-use interactions vary with species combinations, soil-water availability, cropping configuration, and irrigation regime (Chen et al., 2023; Durodola et al., 2025; Hao et al., 2026; O'Connor et al., 2024).

Since the 1950s, numerous shelterbelts dominated by poplar have been established in the Minqin Oasis, where they now constitute an important landscape unit. Nevertheless, the limited diversity of tree species, reduced winter and spring protection, high transpiration demand, and competition between agriculture and forestry for water constrain the performance of these shelterbelts. We therefore investigated a maize-poplar farmland-shelterbelt system in Datan Township using stable hydrogen and oxygen isotopes. The study addressed two questions: (1) how does irrigation water infiltrate and move between farmland and the shelterbelt, and (2) how strongly do maize and poplar overlap in their use of water sources? By estimating water exchange and plant water-source overlap, this study provides evidence to guide tests of irrigation-water allocation in farmland–shelterbelt and agroforestry systems in water-limited regions.

https://doi.org/10.5194/egusphere-2026-4760
Preprint. Discussion started: 21 August 2026

2. Materials and methods

2.1. Site description

Minqin Oasis is located in the lower reaches of the Shiyang River in the Hexi Corridor, Gansu Province (38°27′10″-39°06′53″ N, 102°53′16″-103°49′00″ E; Fig. 1a, b). The region has a temperate continental arid-desert climate characterized by cold winters, hot summers, low precipitation, and high evaporative demand. The Shiyang River, the region's only external surface runoff, is essential to the persistence of the oasis (Zhu et al., 2022). The experimental field was located at the Shiyang River Basin Ecological Environment Comprehensive Observation Station of Northwest Normal University in Beidong Village, Datan Township, in the central Minqin Oasis (38.79° N, 103.23° E; 1,348 m a.s.l.; Fig. 1c). The experimental farmland was planted with maize (*Zea mays* L.) and bordered by a shelterbelt dominated by *Populus alba* L., as well as by ridges and roads. The upper 1 m of soil consisted mainly of loam and sandy loam. Maize was sown in late April and harvested in mid- to late September. During the May–September observation periods in 2021 and 2023, mean air temperature, relative humidity, and precipitation were 22.45 °C, 36.89%, and 98.3 mm, respectively (Fig. 1d). The field was surface-irrigated with well water or canal water supplied from Hongyashan Reservoir. In 2021, four irrigation events occurred on 16 June, 26 June, 7 July, and 1 August.

https://doi.org/10.5194/egusphere-2026-4760
Preprint. Discussion started: 21 August 2026

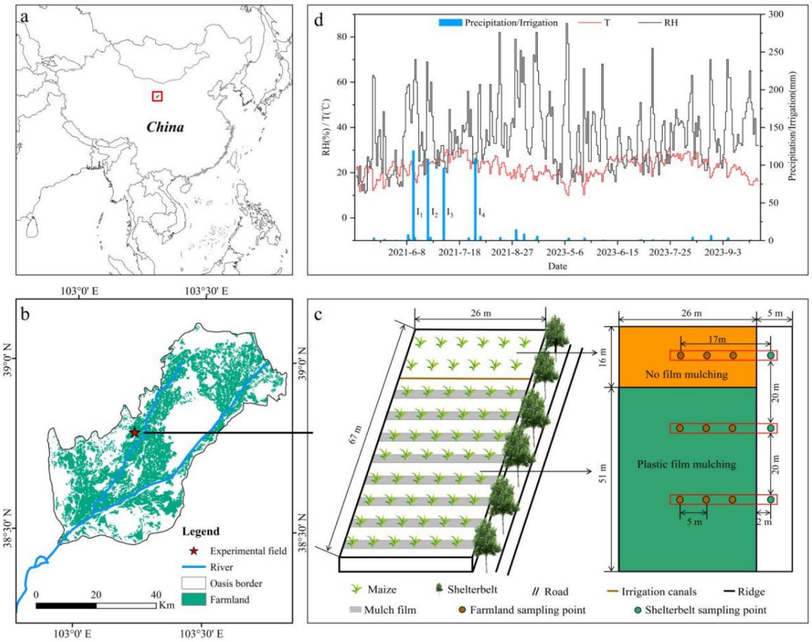

Fig. 1. Location, experimental layout, soil profile, and meteorological conditions of the study area.

2.2. Sampling design

Field sampling was conducted from May to September in 2021 and 2023. The 2021 campaign comprised 876 soil samples and was used to analyze seasonal maize and poplar water sources, monthly water-source overlap, and irrigation-water infiltration, lateral seepage, and transpiration-related exchange during four irrigation events. The 2023 campaign comprised 684 soil samples and focused on spatial variation in soil water and maize water uptake with distance from the shelterbelt. The two annual datasets were analyzed separately and were not pooled for interannual comparison.

Three transects were established across the farmland–shelterbelt interface. Along each transect, farmland samples were collected at 5, 10, and 15 m from the shelterbelt, together with one shelterbelt sampling location. Two transects were located in the film-mulched area and one in the non-mulched area. Fifteen Trime-TDR access tubes were used to monitor soil moisture. Soil was sampled at 10-cm intervals from 0 to 100 cm. Routine sampling was conducted during the growing season, with additional sampling

https://doi.org/10.5194/egusphere-2026-4760
Preprint. Discussion started: 21 August 2026

associated with irrigation and rainfall events. All four irrigation events analyzed in this study occurred in 2021.

2.2.1. Soil sampling

Soil samples were collected from the farmland and shelterbelt at 10-cm depth intervals to a maximum depth of 100 cm. Each sample was divided into two portions. One portion was placed in a 50-mL glass bottle, sealed with Parafilm, and stored at −20 °C for stable-isotope analysis. The other portion was placed in an aluminum box for gravimetric soil-water-content measurement. These two portions originated from the same field sample and were not treated as independent replicates. In total, 1,560 soil samples were collected, comprising 876 samples in 2021 and 684 samples in 2023.

2.2.2. Plant stem and root sampling

Stem samples were rapidly collected from plants near each soil-sampling point, with two parallel samples collected at each sampling event. Samples were placed in 50-mL glass vials, sealed, and frozen at −20 °C until analysis. Plant sampling followed the soil-sampling schedule. Roots were sampled to a depth of 100 cm with a 5-cm-diameter soil auger at 10-cm depth intervals; the sampled volume per interval was approximately 196.25 cm^3. Sampling was conducted only when no precipitation or irrigation had occurred during the preceding 10 days. In the laboratory, soil was passed through a 2-mm sieve and fine roots (<2 mm in diameter) were recovered, weighed fresh, oven-dried, and reweighed.

2.2.3. Water sampling

Precipitation and irrigation water were sampled during each observed event. During the observation period, 20 precipitation events and four irrigation events were recorded. Three replicate samples were collected per event, yielding 72 water samples in total, including 60 precipitation samples and 12 irrigation-water samples. Precipitation was collected with a rain gauge fitted with a funnel and a polyethylene anti-evaporation ball to minimize evaporative isotope fractionation. Immediately after each event, rainwater was transferred to 50-mL high-density polyethylene bottles, sealed with Parafilm, and stored at 0–4 °C until analysis. Irrigation water was collected and stored using the same

https://doi.org/10.5194/egusphere-2026-4760
Preprint. Discussion started: 21 August 2026

procedure. After sample screening and quality control, 60 samples were retained for isotope analysis.

2.2.4. Meteorological data collection

An automatic meteorological station (WatchDog 2000 Series) installed in the experimental field continuously recorded air temperature and relative humidity. Solar radiation, wind speed, and actual vapor pressure were obtained from the Minqin station of the China Meteorological Administration network.

2.3. Methods

2.3.1. Sample analysis

The δ^2H and $\delta^{18}O$ values of precipitation and irrigation water were measured in the Stable Isotope Laboratory of Northwest Normal University using a liquid-water isotope analyzer (DLT-100, Los Gatos Research, Mountain View, CA, USA). Before analysis of maize and poplar stem water and soil water, water was extracted from stems and soil with a low-temperature vacuum-condensation system (LI-2100, Beijing LICA United Technology Co., China). Each water sample and isotope standard was injected six times. To reduce memory effects, the first two injections were discarded and the mean of the final four injections was used (Qiu et al., 2023b). Isotope values are reported in per mille (‰) relative to Vienna Standard Mean Ocean Water (V-SMOW):

$$\delta = \left(\frac{R_{\text{sample}}}{R_{\text{standard}}} - 1\right) \times 1000‰ \quad (1)$$

where R_{sample} is the $^{18}O/^{16}O$ or $^2H/^1H$ ratio of the sample and $R_{standard}$ is the corresponding ratio in V-SMOW. Analytical precision was ±0.6‰ for δ^2H and ±0.2‰ for $\delta^{18}O$.

2.3.2. IsoSource model

Under isotope mass-conservation principles, the proportional contributions of potential water sources were estimated by comparing the stable-isotope compositions of soil water and plant xylem water (Phillips and Gregg, 2003; Sternberg and Swart, 1987). The IsoSource model was used to estimate the contributions of soil water from the surface (0–20 cm), middle (20–60 cm), and deep (60–100 cm) layers. The governing equations were:

https://doi.org/10.5194/egusphere-2026-4760
Preprint. Discussion started: 21 August 2026

$$\delta_s = f_1\delta_1 + f_2\delta_2 + f_3\delta_3 \quad (2)$$

$$1 = f_1 + f_2 + f_3 \quad (3)$$

where δ_1, δ_2, and δ_3 are the isotope values of soil water in the surface (0–20 cm), middle (20–60 cm), and deep (60–100 cm) layers, respectively; δs is the isotope value of plant xylem water; and f_1, f_2, and f_3 are the corresponding source fractions.

2.3.3. Infiltration and lateral seepage of irrigation water

Irrigation-water infiltration and lateral transfer within the farmland–shelterbelt system were estimated using water-balance and isotope mass-conservation equations. We assumed that rainfall and irrigation water did not undergo isotope fractionation upon entry into the soil. After irrigation, water stored in farmland soil layer i was treated as the sum of antecedent storage in that layer and infiltration from the overlying layer. The maximum lateral distance of irrigation water entering the shelterbelt was identified from the soil-moisture access tubes. Water stored in shelterbelt layer i after irrigation was treated as the sum of antecedent storage and lateral seepage from the corresponding farmland layer. A layerwise mass-balance formulation was first applied to vertical infiltration within the farmland profile and was subsequently extended to represent lateral transfer from farmland to the corresponding shelterbelt layer (Yang et al., 2015); the lateral formulation was not independently validated and therefore provides a model-based estimate:

$$\begin{cases} W_{ai} = W_{bi} + F_{i-1} \\ W_{ci} = W_{di} + F_i \end{cases} \quad (4)$$

where W_{ai} and W_{bi} are water storage in farmland layer i after and before irrigation, respectively; W_{ci} and W_{di} are water storage in shelterbelt layer i after and before lateral seepage, respectively; F_{i-1} is infiltration from the overlying layer; and F_i is lateral seepage from farmland layer i to the corresponding shelterbelt layer. Applying isotope mass conservation gives:

$$\begin{cases} \delta_{ai} W_{ai} = \delta_{bi} W_{bi} + \delta_{i-1} F_{i-1} \\ \delta_{ci} W_{ci} = \delta_{di} W_{di} + \delta_i F_i \end{cases} \quad (5)$$

https://doi.org/10.5194/egusphere-2026-4760
Preprint. Discussion started: 21 August 2026

where δ_{ai}, δ_{bi}, and δ_{i-1} are the isotope compositions of farmland soil water in layer i after irrigation, farmland soil water in that layer before irrigation, and water infiltrating from the overlying layer, respectively; δ_{ci}, δ_{di}, and δ_i are the isotope compositions of shelterbelt soil water in layer i after seepage, shelterbelt soil water in that layer before seepage, and farmland soil water supplying lateral seepage, respectively. Rearranging Eqs. (4) and (5) gives the fractions of post-irrigation layer storage attributed to newly infiltrated or laterally transferred water:

$$\begin{cases} \dfrac{F_{i\text{-}1}}{W_{ai}} = \left(\dfrac{\delta_{ai} - \delta_{bi}}{\delta_{i\text{-}1} - \delta_{bi}}\right) \times 100\% \\ \dfrac{F_{i}}{W_{ci}} = \left(\dfrac{\delta_{ci} - \delta_{di}}{\delta_{i} - \delta_{di}}\right) \times 100\% \end{cases} \tag{6}$$

Thus, isotope-based infiltration and lateral-transfer fractions were estimated for each soil layer from the isotope compositions of the component waters. For i = 1, δ_{i-1} denotes the isotope composition of irrigation water. This simplified two-component balance did not separately resolve evaporation, transpiration, drainage below the analyzed layer, preferential flow, or other omitted fluxes. In addition, no common reference-area conversion between the farmland and shelterbelt was documented. The lateral-transfer percentages should therefore be interpreted as irrigation-depth-normalized model estimates rather than area-integrated fractions of the total irrigation volume.

2.3.4. Proportional similarity index (PS)

The proportional similarity (PS) index describes similarity in relative resource-use profiles between two organisms. Higher values indicate greater overlap in proportional resource use, whereas lower values indicate greater partitioning; the index does not by itself measure competitive effects (Trogisch et al., 2016). We used the PS index to quantify overlap in water-source use between maize and poplar:

$$PS = 1 - 0.5\sum_{i=1}^{n}\left|P_{1i} - P_{2i}\right| \tag{7}$$

where P_{1i} and P_{2i} are the proportional contributions of water source i to the two plant species, respectively.

https://doi.org/10.5194/egusphere-2026-4760
Preprint. Discussion started: 21 August 2026

2.3.5. Fine root biomass

The formula for calculating fine root biomass (McClaugherty et al., 1982) is:

$$\mathrm{FRB_i} = \mathrm{W_d} \times 10^4 / \pi (\mathrm{d}/2)^2 \quad (8)$$

where FRB_i is fine-root biomass in a soil layer (g m^{-2}), W_d is root dry mass (g), π is the mathematical constant, and d is the 5-cm inner diameter of the soil auger. The percentage of fine root biomass (PFRB) is:

$$\mathrm{PFRB} = \mathrm{FRB_i}/\mathrm{FRB} \quad (9)$$

where FRB is total fine-root biomass (g m^{-2}).

2.3.6. FAO-56 Penman-Monteith equation

The FAO-56 Penman-Monteith equation was used to estimate reference evapotranspiration (ET_0). Because ET_0 represents a well-watered reference surface, vegetation-specific evapotranspiration requires an appropriate adjustment for canopy and water-stress conditions. ET_0 was calculated using the FAO-56 Penman–Monteith equation (Allen et al., 1998):

$$ET_0 = \frac{0.408\Delta(R_n - G) + \gamma \frac{900}{T+273} U_2 (e_s - e_a)}{\Delta + \gamma(1 + 0.34U_2)} \quad (10)$$

where ET_0 is reference evapotranspiration (mm d^{-1}); R_n is net radiation at the reference surface (MJ m^{-2} d^{-1}); G is soil heat flux (MJ m^{-2} d^{-1}); γ is the psychrometric constant (kPa °C^{-1}); Δ is the slope of the saturation-vapor-pressure curve (kPa °C^{-1}); U_2 is wind speed at 2 m (m s^{-1}); e_s and e_a are saturation and actual vapor pressure (kPa), respectively; and T is mean daily air temperature (°C).

Net radiation was calculated as:

$$R_n = R_{ns} - R_{nl} \quad (11)$$

where R_{ns} and R_{nl} are net shortwave and net longwave radiation, respectively.

$$R_{ns} = (1 - \alpha) \times R_s \quad (12)$$

where R_s is observed incoming solar radiation and α is albedo (0.23 for the reference surface).

https://doi.org/10.5194/egusphere-2026-4760
Preprint. Discussion started: 21 August 2026

Longwave radiation is proportional to the fourth power of the absolute surface temperature and can be quantitatively expressed by the Stefan-Boltzmann law. The calculation formula is as follows:

$$R_{nl} = \sigma\left[\frac{T^4{}_{\max,k} + T^4{}_{\min,k}}{2}\right] \times \left(0.34 - 0.14\sqrt{e_a}\right) \times \left(1.35\frac{R_s}{R_{so}} - 0.35\right) \quad (13)$$

where σ is the Stefan-Boltzmann constant, which is 4.903 × 10^{-9} MJ K^{-4} m^{-2} d^{-1}; $T^4_{max,k}$ and $T^4_{min,k}$ are maximum and minimum absolute temperature (K) in the calculation period, respectively. R_s/R_{so} is relative shortwave radiation; R_s is solar radiation; R_{so} is clear-sky radiation.

Soil heat flux (G) was calculated as:

$$G = \lambda \times \left(\frac{\Delta T}{\Delta Z}\right) \quad (14)$$

where λ is soil thermal conductivity (W m^{-1} K^{-1}), ΔT is the temperature difference between the two measurement depths (K), and ΔZ is their vertical separation (m).

$$\lambda = \lambda_{dry} + \left(\lambda_{sat} - \lambda_{dry}\right) \times \left(\theta / \theta_{sat}\right)^n \quad (15)$$

Here, λ_{dry} and λ_{sat} are the thermal conductivities of dry and saturated soil, respectively; θ and θ_{sat} are volumetric and saturated soil-water content; and n is an empirical shape parameter. Values of these parameters depend on soil texture and must be specified for the study soil.

Other auxiliary variables required in the FAO-56 Penman–Monteith calculation were determined following the standard procedures described by Allen et al. (1998). Solar radiation (R_s), wind speed at 2 m (U_2), actual vapor pressure (e_a), atmospheric pressure (P), and mean daily temperature (T) were obtained from field observations and the Minqin meteorological station. Following the near-versus-far comparison design of Xiao and Huang, (2016), we treated the difference in modeled evapotranspiration between shelterbelt-edge trees and trees farther from the field as a proxy for transpiration-related water exchange. Unlike Xiao and Huang (2016), no sap-flow measurements were available in the present study; this quantity is therefore not a direct

https://doi.org/10.5194/egusphere-2026-4760
Preprint. Discussion started: 21 August 2026

measurement of farmland-water uptake and depends on the stated between-group comparability assumptions.

3. Results

3.1. Modeled transpiration-related water exchange by the shelterbelt

Four monitoring windows associated with irrigation events were analyzed: I (13–20 June 2021; 119 mm), II (24 June–1 July 2021; 108 mm), III (6–13 July 2021; 96 mm), and IV (30 July–6 August 2021; 109 mm), for a total of 432 mm. Across the four event windows, modeled evapotranspiration was 249.20 mm for shelterbelt trees at the farmland edge and 164.71 mm for trees farther from the farmland (Fig. 2). Except during event I, modeled evapotranspiration was relatively high early in each event window, declined as irrigation water infiltrated and moved laterally, and then increased later in the window. One possible explanation is that late-event percolation supplied water below 1 m that remained accessible to trees at the farmland edge.

Across the four monitoring windows, modeled evapotranspiration at the shelterbelt edge exceeded that at the farther location by 84.49 mm (17.25, 17.74, 27.56, and 21.94 mm for windows I–IV, respectively). The numerical ratio of this difference to total applied irrigation was 19.56%; however, because the windows included pre-irrigation days, the difference cannot yet be interpreted as irrigation-water uptake (Table 1). The largest estimate occurred during event III (27.56 mm), coinciding with high July temperatures and the period of rapid poplar growth; this correspondence does not by itself establish causation.

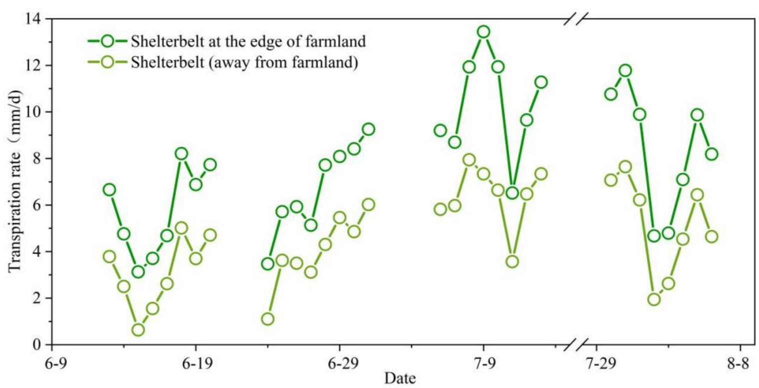

https://doi.org/10.5194/egusphere-2026-4760
Preprint. Discussion started: 21 August 2026

Fig. 2. Modeled evapotranspiration at the shelterbelt edge and at a location farther from the farmland during four irrigation-event windows.

Table 1 Daily modeled evapotranspiration differences between shelterbelt-edge and farther locations during four irrigation-event monitoring windows in 2021.

Irrigation Event I		Irrigation Event II		Irrigation Event III		Irrigation Event IV	
Date	WE (mm)	Date	WE (mm)	Date	WE (mm)	Date	WE (mm)
6-13	2.38	6-24	1.87	7-6	2.88	7-30	3.19
6-14	1.76	6-25	1.59	7-7	2.22	7-31	3.63
6-15	1.99	6-26	1.93	7-8	3.49	8-1	3.17
6-16	1.65	6-27	1.51	7-9	5.61	8-2	2.23
6-17	1.57	6-28	2.91	7-10	4.79	8-3	1.66
6-18	2.70	6-29	2.13	7-11	2.45	8-4	2.06
6-19	2.68	6-30	3.06	7-12	2.68	8-5	2.93
6-20	2.53	7-1	2.73	7-13	3.44	8-6	3.05

Note: WE, modeled evapotranspiration difference between shelterbelt-edge and farther locations. Daily values are rounded to two decimal places for presentation.

3.2. Irrigation-water infiltration and lateral exchange between farmland and the shelterbelt

Soil-water movement differed between farmland and shelterbelt units because of contrasts in irrigation, vegetation, soil layering, mulching, and other site conditions. During the four 2021 irrigation events, we used water balance and isotope mass conservation to estimate infiltration and lateral transfer on the first day after irrigation. For events I-IV (119, 108, 96, and 109 mm), respectively, estimated infiltration was 32.3, 24.8, 26.5, and 30.5 mm in the 0-20 cm layer; 28.2, 26.6, 23.1, and 28.3 mm in the 20-60 cm layer; and 31.7, 33.4, 26.2, and 24.9 mm in the 60-100 cm layer. Using soil-water isotope data before and after irrigation, the corresponding model-estimated lateral transfer into the shelterbelt was 4.7, 3.6, 3.1, and 3.8 mm at 0-20 cm; 6.6, 6.4, 5.3, and 5.4 mm at 20-60 cm; and 5.4, 4.6, 3.3, and 5.3 mm at 60-100 cm (Fig. 3).

https://doi.org/10.5194/egusphere-2026-4760
Preprint. Discussion started: 21 August 2026

Across the four irrigation events, the irrigation-depth-normalized infiltration ratios were 26.42 ± 2.02% (28.53 ± 3.01 mm), 24.59 ± 0.86% (26.55 ± 2.10 mm), and 26.93 ± 2.87% (29.05 ± 3.58 mm) for the 0–20, 20–60, and 60–100 cm farmland layers, respectively. Values are unweighted means ± population standard deviations across the four events (n=4). The corresponding irrigation-depth-normalized lateral-transfer ratios into the shelterbelt were 3.50 ± 0.28% (3.80 ± 0.58 mm), 5.49 ± 0.35% (5.93 ± 0.58 mm), and 4.27 ± 0.53% (4.65 ± 0.84 mm) for the 0–20, 20–60, and 60–100 cm layers, respectively. The sum of the three layer-specific mean ratios was 13.26%, indicating that lateral transfer was greatest in the 20–60 cm layer. Because farmland and shelterbelt reference areas were not converted to a common area basis, the 13.26% value represents the sum of irrigation-depth-normalized layer ratios rather than an area-integrated fraction of the total irrigation volume (Fig. 3b).

https://doi.org/10.5194/egusphere-2026-4760
Preprint. Discussion started: 21 August 2026

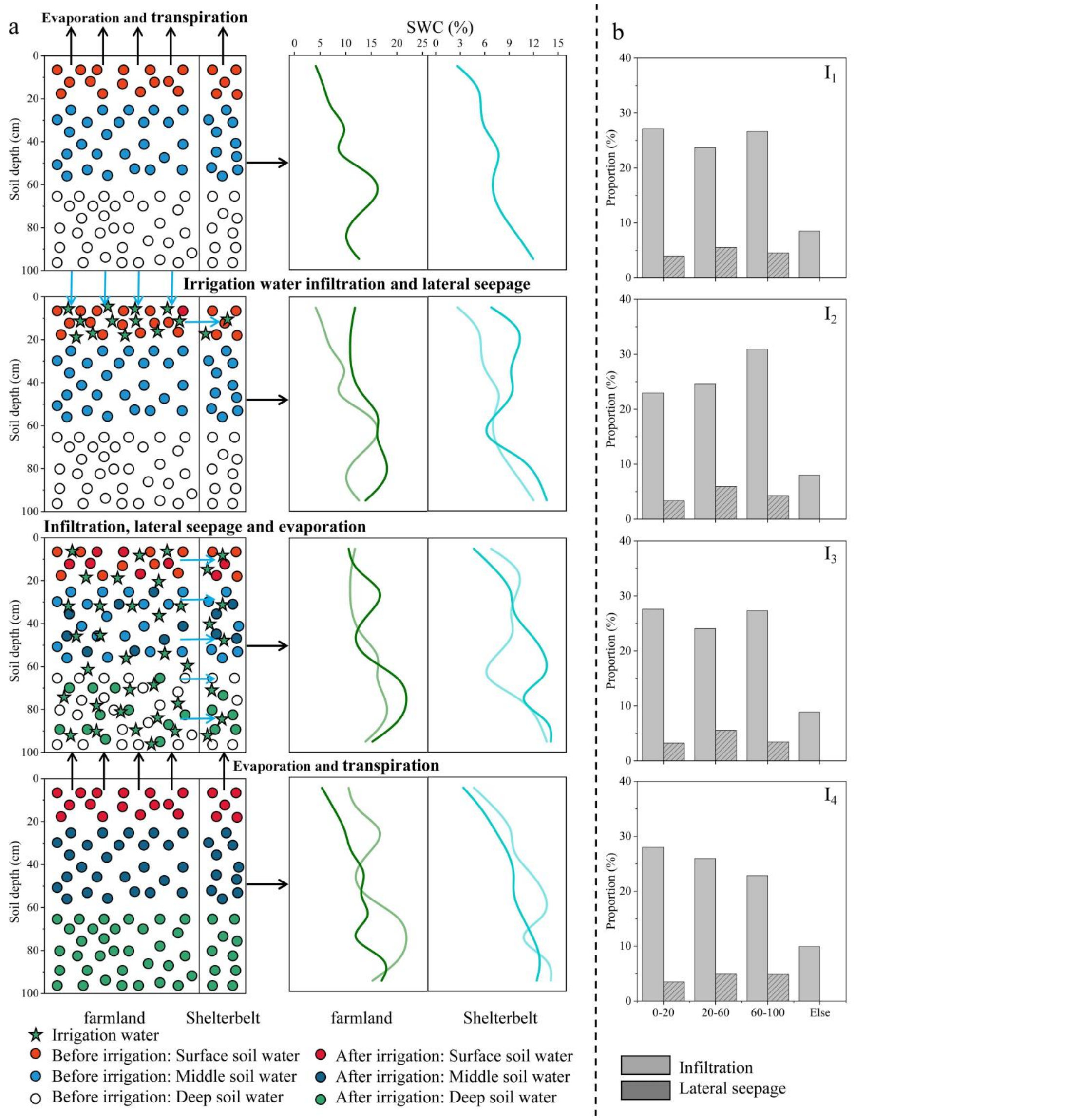

Fig. 3. (a) Conceptual diagram of irrigation-water infiltration and lateral seepage during a single event; pre-irrigation soil-water content is shown in translucent colors. (b) Model-estimated layer-specific infiltration and lateral-transfer fractions on the first day after the four 2021 irrigation events (I_1–I_4).

3.3. Seasonal and spatial variation in plant water sources

Groundwater at the study site was approximately 26 m below ground level (National Groundwater Monitoring Station, Datan Beixin Station), well below the sampled soil

https://doi.org/10.5194/egusphere-2026-4760
Preprint. Discussion started: 21 August 2026

profile; groundwater was therefore assumed to make a negligible direct contribution to the sampled 0–100 cm source domain. Reported maize and poplar source proportions were therefore conditional on the three sampled soil-depth intervals. Across the growing period, maize obtained an estimated 46.38% and 30.04% of its water from the 0-20 and 20-60 cm layers, respectively. Poplar relied more strongly on the 20-60 and 60-100 cm layers, which contributed 29.96% and 47.46%, respectively. Water-source contributions varied seasonally for both species (Fig. 4).

During May and June, maize relied mainly on surface soil water, with estimated contributions of 61.6% and 49.5%, respectively. In July, the estimated contribution of middle-layer water reached its seasonal maximum (33.6%); in August, the contribution of deep-layer water peaked at 36.0%. These shifts coincided with irrigation and root development but do not isolate their individual effects. After irrigation ceased in September, maize again relied mainly on surface soil water, while the 20−60 cm contribution remained 31.9% and the 60−100 cm contribution declined. Across the growing period, surface soil water was the dominant source, with temporary increases in middle- and deep-layer contributions during July and August (Fig. 4a).

In May, surface soil water was the largest estimated source for poplar (43.3%). From June to August, declining reliance on surface water coincided with higher temperature and recharge by rainfall and irrigation. Middle-layer water reached its maximum contribution in June (36.6%), and deep-layer water contributed more than 50% from July onward. The contribution rates of deep soil water from July to September were 50.2%, 58.3%, and 66.9%, respectively. In September, after irrigation ceased and precipitation decreased, the estimated deep-layer contribution reached its seasonal maximum of 66.9% (Fig. 4b). Water-source contributions to maize varied only modestly with distance from the shelterbelt. Surface soil water contributed least to maize 5 m from the shelterbelt (43.5%). With increasing distance from the shelterbelt, the estimated surface-water contribution increased and the deep-soil contribution decreased (Fig. 4c).

https://doi.org/10.5194/egusphere-2026-4760
Preprint. Discussion started: 21 August 2026

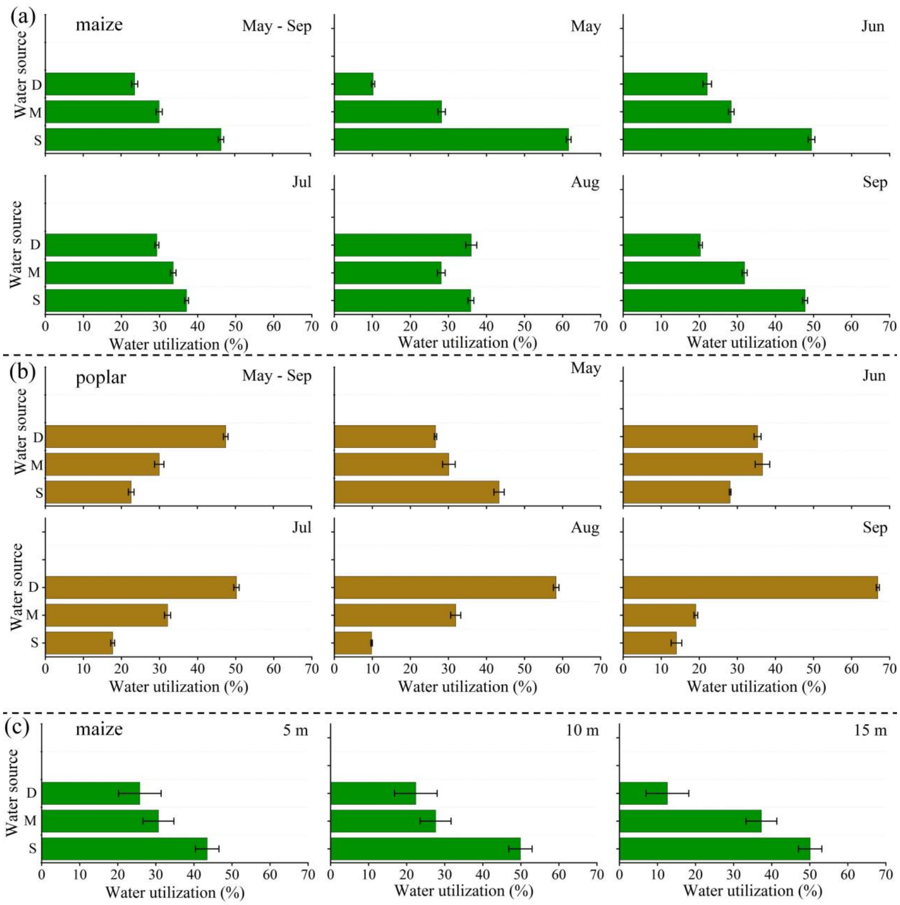

Fig. 4. Estimated soil-water-source contributions to (a) maize, (b) poplar, and (c) maize at 5, 10, and 15 m from the shelterbelt. Error bars indicate variability in the corresponding estimates.

3.4. Water-source overlap between maize and poplar

Across the growing period, the PS index for maize and poplar was 73.35%, indicating substantial overlap in water-source use. The overlap varied by month. It was highest in May (81.7%), when both species relied mainly on surface soil water; the PS index was similar in June and July (78.6% and 79.1%) and then declined in August and September as their estimated source contributions diverged. The lowest PS value occurred in September (53.4%), indicating the greatest seasonal partitioning of water sources (Table 2). Based on the 2023 spatial analysis, the PS index between maize and

https://doi.org/10.5194/egusphere-2026-4760
Preprint. Discussion started: 21 August 2026

poplar decreased with increasing maize distance from the shelterbelt. The index was 78.34% at 5 m, 72.63% at 10 m, and 65.14% at 15 m, with an average of 72.03% across the three distances (Table 3). These results indicate that maize and poplar exhibited the greatest water-source overlap close to the shelterbelt and progressively greater water-source differentiation with increasing distance.

Table 2 Monthly proportional similarity (PS) index for maize and poplar water-source use

Month	5	6	7	8	9	Average
PS index (%)	81.7	78.6	79.1	73.95	53.4	73.35

Table 3 Proportional similarity (PS) index between poplar and maize water-source use at different distances from the shelterbelt during the 2023 transect campaign.

Distance from shelterbelt (m)	5	10	15	Average
PS index (%)	78.34	72.63	65.14	72.03

4. Discussion

4.1. Fine-root distribution and water-source overlap in the farmland–shelterbelt system

Fine roots are the principal organs through which plants acquire soil water and nutrients. In farmland-shelterbelt systems, their distribution can respond to irrigation, canal leakage, rainfall, groundwater, and soil texture (Zhang et al., 2016). Maize and poplar roots at the study site extended to at least 1 m, but their vertical distributions differed. Both species had most fine-root biomass in the upper profile: 60.45% of maize fine roots occurred at 0-20 cm, 24.85% at 20–40 cm, and 58.83% of poplar fine roots at 0-40 cm (Fig. 5). Fine-root biomass generally declined with depth, although poplar showed a slight increase in deeper layers. This pattern may reflect irrigation-derived water and nutrient supply at depth, but the available observations do not isolate that mechanism (Ma et al., 2012; Shen et al., 2014; Woodall and Ward, 2002). Maize fine roots were concentrated at 0-40 cm from May to June and extended deeper after mid-July. Poplar fine-root biomass increased rapidly from May to June and stabilized or

https://doi.org/10.5194/egusphere-2026-4760
Preprint. Discussion started: 21 August 2026

declined from August to September (Coleman et al., 2000). The strong overlap of maize and poplar fine roots in cultivated surface soil provides a plausible basis for the high water-source overlap observed in May and June. Comparable PS values (0.69–0.97) have been reported where coexisting species predominantly used shallow soil water in a semiarid agroforestry system (Chen et al., 2023), although differences in vegetation and soil conditions limit direct comparison. Artificial ^2H_2O labeling in an alley-cropping system likewise showed that young trees and wheat can share soil water in a wet year, underscoring the context dependence of tree–crop water interactions (O’Connor et al., 2024). Recent in situ monitoring of soil and xylem water isotopes in *Salix alba* also demonstrated that the relative use of shallow and deeper soil-water sources can vary over the growing season (Landgraf et al., 2022), although the riparian setting differs from the present arid oasis system.

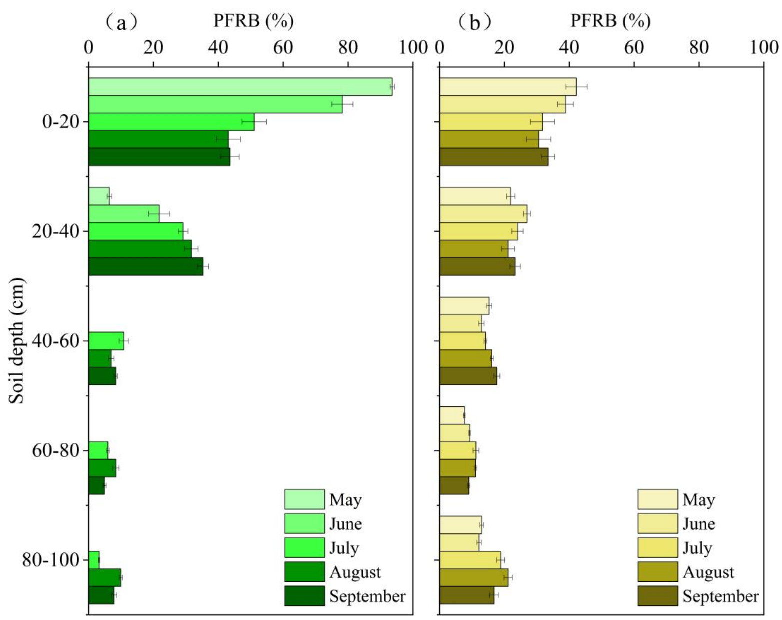

Fig. 5. Vertical distribution of fine-root biomass percentages in (a) farmland maize and (b) shelterbelt poplar. Error bars indicate variability in the corresponding estimates.

4.2. Water-use patterns and implications for irrigation management

https://doi.org/10.5194/egusphere-2026-4760
Preprint. Discussion started: 21 August 2026

The model-estimated transfer of irrigation water from farmland to the shelterbelt suggests a potential trade-off in allocating a limited water supply. Under current practice, local farmers irrigate crops but not shelterbelts, leaving shelterbelt trees dependent partly on water originating in the field. Irrigation management should therefore consider the root-zone requirements of both components while keeping total seasonal water use unchanged or lower. An efficient schedule should replenish root-zone deficits while minimizing deep percolation (Zhang et al., 2016). Maize obtained most of its water from the upper 0.6 m, whereas the mean contribution from 60-100 cm was 23.58% (Fig. 4a). Recent stable-isotope evidence from hyper-arid oasis farmland also showed growth-stage-dependent shifts in maize root water uptake across soil depths and contributions from irrigation water, highlighting the importance of matching irrigation depth to crop water-use dynamics (Zhang et al., 2022). Because flood irrigation at the same Minqin site can move irrigation water and precipitation below 1.0 m (Wang et al., 2023), reducing the maize wetting depth toward 0.6 m may reduce deep percolation. A total of 116.2 mm was estimated to enter the 60–100 cm layer across the four events, but the fraction that could be saved without reducing maize water uptake cannot be determined from these data. Field trials are needed before treating any part of this layer storage as water savings, reallocating it to shelterbelts, or adopting staggered irrigation.

Micro-irrigation delivers water and nutrients near crop roots through pipelines and emitters (Madramootoo and Morrison, 2013). Mulched drip irrigation combines precise water delivery with reduced soil evaporation and may allow smaller, more frequent applications (Li et al., 2019; Ning et al., 2021). Because maize and poplar relied strongly on surface soil water in May and June, smaller and more frequent applications, scheduled separately for farmland and shelterbelts, warrant testing. During July and August, irrigation could be adjusted to maintain a maize wetting depth near 0.6 m, with shallower or no irrigation after harvest. Deeper irrigation of poplar in July and August may also be evaluated. These recommendations should be treated as testable management hypotheses because the present study did not experimentally compare irrigation schedules.

https://doi.org/10.5194/egusphere-2026-4760
Preprint. Discussion started: 21 August 2026

4.3. Implications for poplar shelterbelt design in arid farmland

Farmland shelterbelts are an important component of oasis agroecosystems in arid regions. Poplars (Populus spp.) are widely used because they grow rapidly, are readily propagated, and provide economic and protective benefits. Their rapid growth, however, can entail high water demand, making soil-water availability a major constraint in arid and semi-arid environments (Hogg et al., 2013; Xi et al., 2016, 2017). Poplar roots can extend beyond the crown; reported horizontal and vertical extents vary substantially among species, stand ages, and site conditions (Puri et al., 1994). Dense roots in the upper 0-80 cm may overlap with crop roots and increase competition for water and nutrients. Potential mitigation measures include adjusting shelterbelt density and structure and evaluating alternative species. Recent measurements in poplar–maize systems in the Hexi Corridor indicate that the depth and spatial extent of competition differ between drip and flood irrigation, reinforcing the need to match shelterbelt design to irrigation mode (Hao et al., 2026). A graded grass-shrub-tree arrangement near field margins may reduce direct crop-tree root overlap while retaining wind protection, but this design requires field validation. Future comparative trials should prioritize locally adapted species and evaluate crown geometry, rooting depth, lateral root spread, and protective performance together. Taken together, the results indicate that irrigation links maize cropland and the adjacent poplar shelterbelt through multiple pathways (Fig. 6). Irrigation water infiltrates vertically through the farmland soil profile and is partly transferred laterally toward the shelterbelt, particularly through the middle soil layer. At the same time, the contrasting root distributions of maize and poplar allow the two species to use different portions of the soil profile, although substantial water-source overlap remains, especially near the shelterbelt and during the early growing season. These coupled hydrological and root-mediated processes suggest that irrigation management and shelterbelt design should be considered jointly rather than as independent components of the oasis agroecosystem.

https://doi.org/10.5194/egusphere-2026-4760
Preprint. Discussion started: 21 August 2026

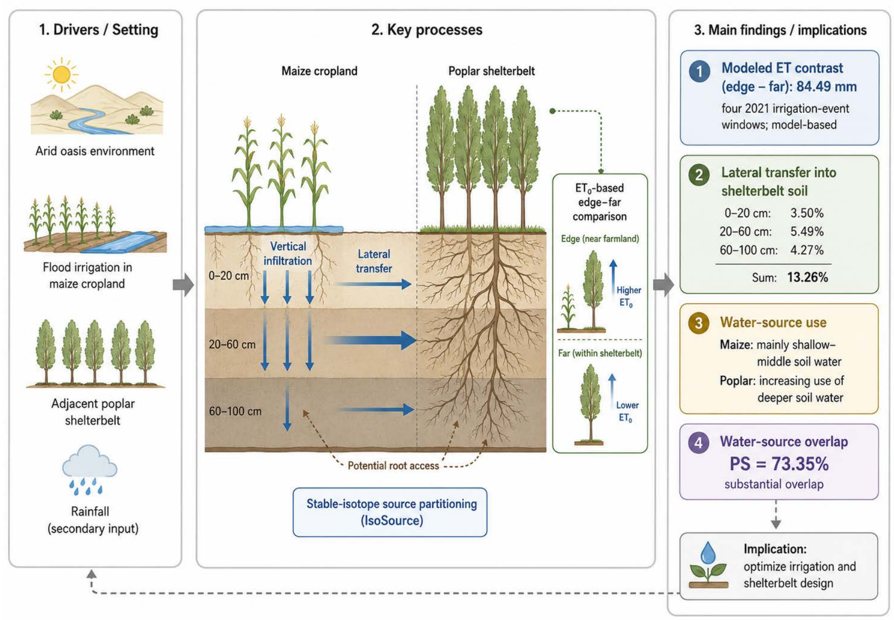

Fig. 6. Conceptual framework of irrigation-water redistribution and maize–poplar water-use interactions in the farmland–shelterbelt system.

4.4. Limitations and priorities for future work

Water exchange between farmland and shelterbelts may involve lateral seepage of irrigation water (Karray et al., 2008), uptake of farmland soil water by tree roots extending into fields (Shen et al., 2014), and groundwater-driven exchange (Yi et al., 2015). We estimated lateral seepage using stable isotopes and a mass-balance framework. Because direct sap-flow observations were unavailable, root-mediated uptake from farmland was inferred from the difference in modeled evapotranspiration between trees at the farmland edge and trees farther away. This estimate depends on the assumption that location-related differences in modeled evapotranspiration primarily reflect access to farmland water rather than microclimatic, structural, or physiological differences between tree groups. Groundwater exchange was assumed to be negligible because the National Groundwater Monitoring Station at Datan Beixin Station recorded a water-table depth of approximately 26 m, substantially below the sampled rooting and irrigation-infiltration depths. In addition, grouping soil water into three broad layers and summarizing IsoSource solutions can mask within-layer isotope

https://doi.org/10.5194/egusphere-2026-4760
Preprint. Discussion started: 21 August 2026

heterogeneity and endmember overlap (Rothfuss and Javaux, 2017). Recent studies further indicate that natural-abundance stable-isotope approaches may overestimate deep-layer soil-water use when the active uptake depth is not independently constrained (Wang et al., 2022), and that the choice of isotope mixing model can affect estimated source proportions (Qiu et al., 2025). Stable-isotope approaches are also increasingly used to partition evapotranspiration and quantify evaporation and transpiration under field conditions (Liebhard et al., 2022), whereas tree transpiration is commonly measured using tracers, thermal-dissipation probes, or micrometeorological methods (Drexler et al., 2004; Dye et al., 1992; Smith and Allen, 1996). Micrometeorological approaches are difficult to apply over heterogeneous surfaces (Bambach et al., 2022). Future work should therefore combine stable-isotope measurements with sap-flow observations, such as thermal-dissipation probes, to test the model-based exchange estimate, quantify its uncertainty, and resolve the timing and magnitude of farmland water uptake by shelterbelt roots.

5. Conclusion

This study investigated irrigation-water redistribution and water-use interactions between maize cropland and poplar shelterbelts in the Minqin Oasis using stable hydrogen and oxygen isotopes, isotope mass balance, the Penman–Monteith model, IsoSource, and the proportional similarity index. The results showed that farmland irrigation water was transferred to the shelterbelt through two complementary pathways: lateral movement through the soil profile and potential uptake by shelterbelt roots extending toward the farmland.

Across the four irrigation-event monitoring windows in 2021, modeled evapotranspiration at the shelterbelt edge exceeded that at the farther location by 84.49 mm, equivalent to 19.56% of the total applied irrigation depth. Because the monitoring windows included pre-irrigation days and the estimates were not independently validated by sap-flow measurements, this value should be interpreted as a model-estimated transpiration-related exchange rather than a direct measurement of irrigation-water uptake. On the first day after irrigation, the irrigation-depth-normalized lateral-transfer ratios into the 0–20, 20–60, and 60–100 cm shelterbelt soil layers were 3.50%, 5.49%, and 4.27%, respectively, yielding a summed layer-specific ratio of 13.26%. The largest lateral-transfer ratio occurred in the 20–60 cm layer, indicating that the middle soil layer was an important pathway for irrigation-water redistribution.

Maize relied primarily on surface and middle soil water, whereas poplar increasingly used deeper soil water as the growing season progressed. Nevertheless, the two species exhibited substantial overlap in their proportional use of soil-water sources, with a mean PS index of 73.35%. This overlap was greatest during the early growing season and declined toward September as their water-use patterns became more differentiated. Overall, the farmland–shelterbelt system exhibited a coupled process of irrigation-water redistribution and overlapping plant water use. Optimizing irrigation depth and timing, coordinating water supply between farmland and shelterbelts, and adjusting shelterbelt structure or tree-species composition may improve water-use efficiency and reduce crop–tree water competition in arid oasis agroecosystems. These management implications require further validation through controlled irrigation and sap-flow experiments.

Conflict of Interest Statement

The authors declare no conflicts of interest.

Author contribution

Xinyue Wang and Dongdong Qiu contributed equally to this work and drafted the manuscript. Guofeng Zhu conceived and supervised the study. Yuanfeng Liu contributed to the analysis of management implications and reviewed and edited the manuscript. Rui Li, Zhijie Zheng, and Ru Ma analyzed the data. Wenzhang Sun, Yaxin Li, and Dongfei Yang prepared the figures. Yitian Lei was responsible for manuscript submission.

Funding:

This research was financially supported by the National Natural Science Foundation of China (42371040), the Key Natural Science Foundation of Gansu Province (23JRRA698), the Western Light Young Scholars Program of the Chinese Academy of Sciences (25JR6KA001),the Key Research and Development Program of Gansu Province (22YF7NA122), the Gansu Provincial Basic Research Innovaion Group

https://doi.org/10.5194/egusphere-2026-4760
Preprint. Discussion started: 21 August 2026

Project (22JR5RA129), the Water Resources Science Experimental Research and Technology Promotion Project of Gansu Provincial (25GSLK062), the Cultivation Program of Major key projects of Northwest Normal University (NWNU-LKZD-202302), the Oasis Scientific Research achievements Breakthrough Action Plan Project of Northwest normal University (NWNU-LZKX-202303), the Special Project on Rural Revitalization and Food Security of the Ministry of Agriculture and Rural Affairs. The Gansu Provincial Water Conservancy Science and Technology Promotion Program project "Analysis of the Spatiotemporal Characteristics of Precipitation over the Past 50 Years in the Longzhong and Longdong Loess Plateau Region" (Gan Shui Jian Guan Fa [2021] No.71-20)

Data Availability Statement

The data that support the findings of this study are available on request from the corresponding author.

References:

Allen, R. G., Pereira, L. S., Raes, D., and Smith, M.: Crop evapotranspiration-Guidelines for computing crop water requirements-FAO Irrigation and drainage paper 56, Fao, rome, 300, D05109, 1998.

Bambach, N., Kustas, W., Alfieri, J., Prueger, J., Hipps, L., McKee, L., Castro, S. J., Volk, J., Alsina, M. M., and McElrone, A. J.: Evapotranspiration uncertainty at micrometeorological scales: the impact of the eddy covariance energy imbalance and correction methods, Irrigation Science, 40, 445–461, 2022.

Bowen, G. J., Cai, Z., Fiorella, R. P., and Putman, A. L.: Isotopes in the water cycle: regional-to global-scale patterns and applications, Annual Review of Earth and Planetary Sciences, 47, 453–479, 2019.

Brandle, J. R., Hodges, L., and Zhou, X. H.: Windbreaks in North American agricultural systems, Agroforestry systems, 61, 65–78, 2004.

Chen, Z., Wang, G., Yang, X., Li, Z., and Shen, Y.: Water competition among the coexisting Platycladus orientalis, Prunus davidiana and Medicago sativa in a semi-arid agroforestry system, Agricultural Water Management, 279, 108206, 2023.

https://doi.org/10.5194/egusphere-2026-4760
Preprint. Discussion started: 21 August 2026

Coleman, M. D., Dickson, R. E., and Isebrands, J. G.: Contrasting fine-root production, survival and soil CO2 efflux in pine and poplar plantations, Plant and Soil, 225, 129–139, 2000.

Drexler, J. Z., Snyder, R. L., Spano, D., and Paw U, K. T.: A review of models and micrometeorological methods used to estimate wetland evapotranspiration, Hydrological processes, 18, 2071–2101, 2004.

Durodola, O. S., Rothfuss, Y., Hawes, C., Smith, J., Valentine, T. A., and Geris, J.: Stable water isotopes reveal modification of cereal water uptake strategies in agricultural co-cropping systems, Agriculture, Ecosystems & Environment, 381, 109439, 2025.

Dye, P. J., Olbrich, B. W., and Calder, I. R.: A comparison of the heat pulse method and deuterium tracing method for measuring transpiration from Eucalyptus grandis trees, Journal of Experimental Botany, 43, 337–343, 1992.

Fischer, J., Zerger, A., Gibbons, P., Stott, J., and Law, B. S.: Tree decline and the future of Australian farmland biodiversity, Proceedings of the National Academy of Sciences, 107, 19597–19602, 2010.

Hao, Y., Xi, H., Cheng, W., Yu, T., Li, B., Han, T., Chen, Y., Qu, L., and Wang, Z.: Mechanism of water and nutrient competition between shelterbelts and farmland under different irrigation patterns in the Hexi Corridor oasis area, China, Soil and Tillage Research, 263, 107284, 2026.

Hogg, E. H., Barr, A. G., and Black, T. A.: A simple soil moisture index for representing multi-year drought impacts on aspen productivity in the western Canadian interior, Agricultural and Forest Meteorology, 178, 173–182, 2013.

Huang, X., Yu, Z., Qian, W., Xu, D., and Ai, G.: Effects of adding water on seasonal variation of soil nitrogen availability under sandy grasslands in semi-arid region, Journal of Forestry Research, 18, 287–290, 2007.

Iwasaki, K., Torita, H., Abe, T., Uraike, T., Touze, M., Fukuchi, M., Sato, H., Iijima, T., Imaoka, K., and Igawa, H.: Spatial pattern of windbreak effects on maize growth evaluated by an unmanned aerial vehicle in Hokkaido, northern Japan, Agroforestry Systems, 93, 1133–1145, 2019.

https://doi.org/10.5194/egusphere-2026-4760
Preprint. Discussion started: 21 August 2026

Kanzler, M., Böhm, C., Mirck, J., Schmitt, D., and Veste, M.: Microclimate effects on evaporation and winter wheat (Triticum aestivum L.) yield within a temperate agroforestry system, Agroforestry systems, 93, 1821–1841, 2019.

Karray, J. A., Lhomme, J.-P., Masmoudi, M. M., and Mechlia, N. B.: Water balance of the olive tree–annual crop association: A modeling approach, Agricultural Water Management, 95, 575–586, 2008.

Landgraf, J., Tetzlaff, D., Dubbert, M., Dubbert, D., Smith, A., and Soulsby, C.: Xylem water in riparian willow trees (Salix alba) reveals shallow sources of root water uptake by in situ monitoring of stable water isotopes, Hydrology and Earth System Sciences, 26, 2073–2092, 2022.

Li, M., Du, Y., Zhang, F., Bai, Y., Fan, J., Zhang, J., and Chen, S.: Simulation of cotton growth and soil water content under film-mulched drip irrigation using modified CSM-CROPGRO-cotton model, Agricultural Water Management, 218, 124–138, 2019.

Liebhard, G., Klik, A., Stumpp, C., and Nolz, R.: Partitioning evapotranspiration using water stable isotopes and information from lysimeter experiments, Hydrological Sciences Journal, 67, 646–661, 2022.

Liu, Z., Yu, X., Jia, G., Zhang, J., and Zhang, Z.: Water consumption by an agroecosystem with shelter forests of corn and Populus in the North China Plain, Agriculture, Ecosystems & Environment, 265, 178–189, 2018.

Liu, Z., Jia, G., and Yu, X.: Variation of water uptake in degradation agroforestry shelterbelts on the North China Plain, Agriculture, Ecosystems & Environment, 287, 106697, 2020.

Ma, L., Wu, P., and Wang, Y.: Spatial distribution of roots in a dense jujube plantation in the semiarid hilly region of the Chinese Loess Plateau, Plant and Soil, 354, 57–68, 2012.

Madramootoo, C. A. and Morrison, J.: Advances and challenges with micro-irrigation, Irrigation and Drainage, 62, 255–261, 2013.

McClaugherty, C. A., Aber, J. D., and Melillo, J. M.: The role of fine roots in the organic matter and nitrogen budgets of two forested ecosystems, Ecology, 63, 1481–1490, 1982.

Mueller, N. D., Gerber, J. S., Johnston, M., Ray, D. K., Ramankutty, N., and Foley, J. A.: Closing yield gaps through nutrient and water management, Nature, 490, 254–257, 2012.

Ning, S., Zhou, B., Shi, J., and Wang, Q.: Soil water/salt balance and water productivity of typical irrigation schedules for cotton under film mulched drip irrigation in northern Xinjiang, Agricultural Water Management, 245, 106651, 2021.

O'Connor, C., Choma, C., Ndiaye, A., Delbende, F., Zeller, B., Manouvrier, E., Desmyttère, H., Siah, A., Waterlot, C., and Andrianarisoa, K. S.: Young trees share soil water with wheat in an alley-cropping system in a wet crop year: Evidence from 2H2O artificial labeling, Journal of Hydrology, 635, 131021, 2024.

Penna, D., Geris, J., Hopp, L., and Scandellari, F.: Water sources for root water uptake: Using stable isotopes of hydrogen and oxygen as a research tool in agricultural and agroforestry systems, Agriculture, Ecosystems & Environment, 291, 106790, 2020.

Phillips, D. L. and Gregg, J. W.: Source partitioning using stable isotopes: coping with too many sources, Oecologia, 136, 261–269, 2003.

Puri, S., Singh, V., Bhushan, B., and Singh, S.: Biomass production and distribution of roots in three stands of Populus deltoides, Forest Ecology and Management, 65, 135–147, 1994.

Qiu, D., Zhu, G., Lin, X., Jiao, Y., Lu, S., Liu, J., Liu, J., Zhang, W., Ye, L., and Li, R.: Dissipation and movement of soil water in artificial forest in arid oasis areas: Cognition based on stable isotopes, Catena, 228, 107178, 2023a.

Qiu, D., Zhu, G., Bhat, M. A., Wang, L., Liu, Y., Sang, L., Lin, X., Zhang, W., and Sun, N.: Water use strategy of nitraria tangutorum shrubs in ecological water delivery area of the lower inland river: Based on stable isotope data, Journal of Hydrology, 624, 129918, 2023b.

Qiu, X., Zhang, M., Wang, S., Meng, H., and Che, C.: Comparison of stable isotope mixing models for examining plant root water uptake, PloS one, 20, e0318771, 2025.

Ren, X., Sun, D., and Wang, Q.: Modeling the effects of plant density on maize productivity and water balance in the Loess Plateau of China, Agricultural Water Management, 171, 40–48, 2016.

Rivest, D. and Vézina, A.: Maize yield patterns on the leeward side of tree windbreaks are site-specific and depend on rainfall conditions in eastern Canada, Agroforestry Systems, 89, 237–246, 2015.

Rosa, L., Chiarelli, D. D., Rulli, M. C., Dell'Angelo, J., and D'Odorico, P.: Global agricultural economic water scarcity, Science advances, 6, eaaz6031, 2020.

Rothfuss, Y. and Javaux, M.: Reviews and syntheses: Isotopic approaches to quantify root water uptake: a review and comparison of methods, Biogeosciences, 14, 2199–2224, 2017.

Shen, Q., Gao, G., Fu, B., and Lü, Y.: Soil water content variations and hydrological relations of the cropland-treebelt-desert land use pattern in an oasis-desert ecotone of the Heihe River Basin, China, Catena, 123, 52–61, 2014.

Shen, Q., Gao, G., Hu, W., and Fu, B.: Spatial-temporal variability of soil water content in a cropland-shelterbelt-desert site in an arid inland river basin of Northwest China, Journal of Hydrology, 540, 873–885, 2016.

Smith, D. M. and Allen, S. J.: Measurement of sap flow in plant stems, Journal of experimental Botany, 47, 1833–1844, 1996.

Sternberg, L. da S. L. and Swart, P. K.: Utilization of freshwater and ocean water by coastal plants of southern Florida, Ecology, 68, 1898–1905, 1987.

Tamburini, G., Bommarco, R., Wanger, T. C., Kremen, C., Van Der Heijden, M. G., Liebman, M., and Hallin, S.: Agricultural diversification promotes multiple ecosystem services without compromising yield, Science advances, 6, eaba1715, 2020.

Tan, X., Shao, D., Gu, W., and Liu, H.: Field analysis of water and nitrogen fate in lowland paddy fields under different water managements using HYDRUS-1D, Agricultural Water Management, 150, 67–80, 2015.

Trogisch, S., Salmon, Y., He, J.-S., Hector, A., and Scherer-Lorenzen, M.: Spatio-temporal water uptake patterns of tree saplings are not altered by interspecific

https://doi.org/10.5194/egusphere-2026-4760
Preprint. Discussion started: 21 August 2026

interaction in the early stage of a subtropical forest, Forest Ecology and Management, 367, 52–61, 2016.

Wang, L., Zhu, G., Qiu, D., Liu, Y., Zhao, K., Sang, L., Zhang, Z., Sun, Z., Yong, L., and Jiao, Y.: The use of stable isotopes to determine optimal application of irrigation-water to a maize crop, Plant and Soil, 482, 679–696, 2023.

Wang, S., Gao, X., Yang, M., Huo, G., Song, X., Siddique, K. H., Wu, P., and Zhao, X.: The natural abundance of stable water isotopes method may overestimate deep-layer soil water use by trees, Hydrology and Earth System Sciences Discussions, 2022, 1–22, 2022.

Ward, F. A. and Pulido-Velazquez, M.: Water conservation in irrigation can increase water use, Proceedings of the National Academy of Sciences, 105, 18215–18220, 2008.

Woodall, G. S. and Ward, B. H.: Soil water relations, crop production and root pruning of a belt of trees, Agricultural water management, 53, 153–169, 2002.

Xi, B., Bloomberg, M., Watt, M. S., Wang, Y., and Jia, L.: Modeling growth response to soil water availability simulated by HYDRUS for a mature triploid Populus tomentosa plantation located on the North China Plain, Agricultural Water Management, 176, 243–254, 2016.

Xi, B., Di, N., Wang, Y., Duan, J., and Jia, L.: Modeling stand water use response to soil water availability and groundwater level for a mature Populus tomentosa plantation located on the North China Plain, Forest Ecology and Management, 391, 63–74, 2017.

Xiao, Q. and Huang, M.: Fine root distributions of shelterbelt trees and their water sources in an oasis of arid northwestern China, Journal of Arid Environments, 130, 30–39, 2016.

Xue, J., Gui, D., Lei, J., Sun, H., Zeng, F., Mao, D., Jin, Q., and Liu, Y.: Oasification: An unable evasive process in fighting against desertification for the sustainable development of arid and semiarid regions of China, Catena, 179, 197–209, 2019.

https://doi.org/10.5194/egusphere-2026-4760
Preprint. Discussion started: 21 August 2026

Yang, B., Wen, X., and Sun, X.: Irrigation depth far exceeds water uptake depth in an oasis cropland in the middle reaches of Heihe River Basin, Sci Rep, 5, 15206, https://doi.org/10.1038/srep15206, 2015.

Yi, J., Zhao, Y., Shao, M., Li, H., Jiang, R., Hill, R. L., and Si, B.: Hydrological processes and eco-hydrological effects of farmland–forest–desert transition zone in the middle reaches of Heihe River Basin, Gansu, China, Journal of Hydrology, 529, 1690–1700, 2015.

Zhang, Y., Xiao, Q., and Huang, M.: Temporal stability analysis identifies soil water relations under different land use types in an oasis agroforestry ecosystem, Geoderma, 271, 150–160, 2016.

Zhang, Y., Wu, S., Kang, W., and Tian, Z.: Multiple sources characteristics of root water uptake of crop under oasis farmlands in hyper-arid regions, Agricultural Water Management, 271, 107814, 2022.

Zhao, L. and Zhao, W.: Water balance and migration for maize in an oasis farmland of northwest China, Chinese science bulletin, 59, 4829–4837, 2014.

Zheng, X., Zhu, J., and Xing, Z.: Assessment of the effects of shelterbelts on crop yields at the regional scale in Northeast China, Agricultural Systems, 143, 49–60, 2016.

Zhu, G., Liu, Y., Shi, P., Jia, W., Zhou, J., Liu, Y., Ma, X., Pan, H., Zhang, Y., and Zhang, Z.: Stable water isotope monitoring network of different water bodies in Shiyang River basin, a typical arid river in China, Earth System Science Data Discussions, 2022, 1–23, 2022.